AIAA AVIATION Forum
June 27-July 1, 2022, Chicago, IL & Virtual
AIAA AVIATION 2022 Forum

10.2514/6.2022-3553

Simulation of 3D Co-Flow Jet Airfoil with Integrated Micro-Compressor Actuator

Yan Ren * Paula Alejandra Barrios † Gecheng Zha ‡
Dept. of Mechanical and Aerospace Engineering
University of Miami, Coral Gables, Florida 33124
E-mail: gzha@miami.edu

Abstract

This paper presents the simulations of 3D Co-Flow Jet (CFJ) active flow control airfoil with an integrated micro-compressor. This is an important step to simulate the CFJ flow control airfoil by controlling the RPM of the micro-compressor actuator. The simulations are performed at freestream Mach number 0.3 to simulate the cruise condition of a general aviation electric aircraft. The airfoil used in this work is CFJ-NACA-6421. The simulations employ 3D RANS solver with Spalart-Allmaras (S-A) turbulence model, 3rd order WENO scheme for the inviscid fluxes, and 2nd order central differencing for the viscous terms.

The micro-compressor actuator is designed to achieve high efficiency at a required mass flow rate to maintain a desirable momentum coefficient (C_μ) of the CFJ airfoil at a certain flight condition. The aerodynamic performance, CFJ mass flow rate, energy expenditure, and 3D flow field are studied for the CFJ airfoil at different micro-compressor working points, which is achieved by fixing the compressor RPM and modifying the CFJ airfoil Angles of Attack (AoA). The results show that the compressor mass flow rate linearly increases with the rise of the CFJ airfoil AoA, except at a high AoA of 12°, which leads to the stall of the airfoil. When the AoA increases, the CFJ airfoil stalls before the compressor chokes. The stall of the airfoil decreases the mass flow passing through the compressor, which prevent the compressor from achieving higher mass flow. For the aerodynamic performance of the CFJ airfoil, the maximum C_L/C_D achieved is 122.6. The maximum $(C_L/C_D)_c$ achieved is 52.3, with the compressor efficiency $\eta = 74.3\%$. The simulation results suggest that for large AoA leading to airfoil stall, the compressor RPM need to be increased to move the compressor operating line up to have higher mass flow rate and C_μ. The present study establishes a very important simulation tool, which can mimic the whole CFJ airfoil aerodynamic performance with integrated micro-compressor actuators to control the airfoil within a flight envelop at different operating conditions.

Nomenclature

CFJ	Co-flow jet
AoA	Angle of attack
LE	Leading Edge
TE	Trailing Edge
S	Planform area
s	Wing Span length
c	Profile chord

* Postdoc Researcher, Ph.D., AIAA member
† Ph.D. student, AIAA member
‡ Professor, ASME Fellow, AIAA associate Fellow

U	Flow velocity
q	Dynamic pressure $0.5\,\rho\,U^2$
p	Static pressure
ρ	Air density
$\dot{m}$	Mass flow
M	Mach number
ω	Pitching Moment
P	Pumping power
∞	Free stream conditions
C_L	Lift coefficient $L/(q_\infty\,S)$
C_D	Drag coefficient $D/(q_\infty\,S)$
C_μ	Jet momentum coef. $\dot{m}_j\,U_j/(q_\infty\,S)$
Pc	Power coefficient $L/(q_\infty\,S\,V_\infty)$
η	Micro-compressor total-to-total efficiency
$(C_L/C_D)_c$	CFJ airfoil corrected aerodynamic efficiency $C_L/(C_D+P_c)$

1 Introduction

Co-Flow Jet (CFJ) flow control method [1, 2, 3, 4, 5, 6, 7, 8, 9, 10, 11] is demonstrated to achieve radical lift augmentation, stall margin increase, drag reduction for stationary and pitching airfoils. In the CFJ airfoil concept, an injection slot near the leading edge (LE) and a suction slot near the trailing edge (TE) on the airfoil suction surface are created. As shown in Fig. 1, a small amount of mass flow is withdrawn into the suction duct, pressurized and energized by a micro compressor, and then injected near the LE tangentially to the main flow via a injection duct. The whole process does not add any mass flow to the system and hence is a zero-net mass-flux (ZNMF) flow control. The validity of CFJ flow control method in CFJ-NACA-6421 airfoil is demonstrated in our previous publication [8, 12]. However, the micro compressor interfaces with the injection and suction ducts are simulated by profile boundary conditions extracted from the compressor. The simulation only reflects a specified operating condition of the compressor and does not have any interaction effect between the micro-compressor actuator and the airfoil, which will determine the CFJ wing system operating line (or map) at different flow conditions in a flight envelop such as the variation of angle of attack, flow speed, etc. The aerodynamic performance of CFJ airfoil with micro-compressor actuator integrated need to be studied.

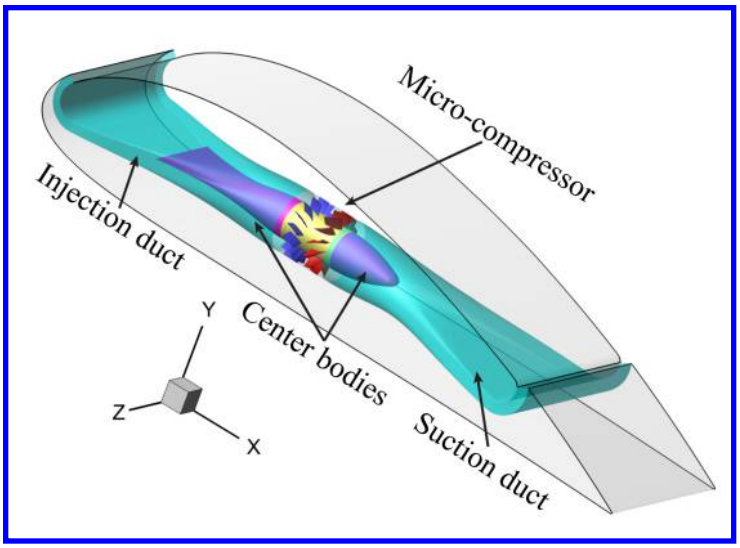

Figure 1: Schematic plot of a typical CFJ airfoil.

The purpose of this paper is to simulate the 3D CFJ active flow control airfoil with an integrated compressor actuator along with suction and injection ducts as a complete system shown in Fig. 1. As indicated in Fig. 1, the suction duct is connected to the micro-compressor actuator inlet and the injection duct is connected to the micro-compressor outlet. The micro-compressor is designed to achieve high efficiency at a specified mass flow rate range, which is required to maintain a desirable momentum coefficient (C_μ) of the CFJ airfoil within a certain range. In order to reduce the energy loss inside the ducts, center-bodies connecting to the inner circles of the micro compressor inlet and outlet are used to guild the flow as shown in Fig. 1. Parametric studies are performed to study the CFJ airfoil and micro-compressor performance at different compressor working points. The conclusion of this work could provide guidance for future high-efficiency CFJ wing aircraft design and control.

2 Methodology

2.1 Lift and Drag Calculation

The momentum and pressure at the injection and suction slots produce a reactionary force, which is automatically measured by the force balance in wind tunnel testing. However, for CFD simulation, the full reactionary force needs to be included. Using control volume analysis, the reactionary force can be calculated using the flow parameters at the injection and suction slot opening surfaces. Zha et al. [2] give the following formulations to calculate the lift and drag due to the jet reactionary force for a CFJ airfoil. By considering the effects of injection and suction jets on the CFJ airfoil, the expressions for these reactionary forces are given as :

$$F_{x_{cfj}} = (\dot{m}_j V_{j1} + p_{j1} A_{j1}) * cos(\theta_1 - \alpha) - (\dot{m}_j V_{j2} + p_{j2} A_{j2}) * cos(\theta_2 + \alpha) \tag{1}$$

$$F_{y_{cfj}} = (\dot{m}_{j1} V_{j1} + p_{j1} A_{j1}) * sin(\theta_1 - \alpha) + (\dot{m}_{j2} V_{j2} + p_{j2} A_{j2}) * sin(\theta_2 + \alpha) \tag{2}$$

where the subscripts 1 and 2 stand for the injection and suction respectively, and θ_1 and θ_2 are the angles between the injection and suction slot's surface and a line normal to the airfoil chord. α is the angle of attack.

The total lift and drag on the airfoil can then be expressed as:

$$D = R'_x - F_{x_{cfj}} \tag{3}$$

$$L = R'_y - F_{y_{cfj}} \tag{4}$$

where R'_x and R'_y are the surface integral of pressure and shear stress in x (drag) and y (lift) direction excluding the internal ducts of injection and suction. For CFJ wing simulations, the total lift and drag are calculated by integrating Eqs.(3) and (4) in the spanwise direction.

2.2 Jet Momentum Coefficient

The jet momentum coefficient C_μ is a parameter used to quantify the jet intensity. It is defined as:

$$C_\mu = \frac{\dot{m} V_j}{\frac{1}{2}\rho_\infty {V_\infty}^2 S} \tag{5}$$

where $\dot{m}$ is the injection mass flow, V_j is the mass-averaged injection velocity, ρ_∞ and V_∞ denote the free stream density and velocity, and S is the planform area. In this study, the CFJ injection momentum coefficient is controlled by the compressor RPM that also determines the compressor power.

2.3 Micro-compressor Power Coefficient

CFJ is implemented by mounting a pumping system inside the wing that withdraws air from the suction slot and blows it into the injection slot. The power consumption is determined by the jet mass flow and total enthalpy change as the following:

$$P = \dot{m}(H_{t1} - H_{t2}) \tag{6}$$

where H_{t1} and H_{t2} are the mass-averaged total enthalpy in the injection cavity and suction cavity respectively, P is the Power required by the pump and $\dot{m}$ the jet mass flow rate. Introducing P_{t1} and P_{t2} the mass-averaged total pressure in the injection and suction cavity respectively, the compressor efficiency η, and the total pressure ratio of the pump $\Gamma = \frac{P_{t1}}{P_{t2}}$, the power consumption is expressed as:

$$P = \frac{\dot{m} C_p T_{t2}}{\eta}(\Gamma^{\frac{\gamma-1}{\gamma}} - 1) \tag{7}$$

where γ is the specific heat ratio equal to 1.4 for air. The power coefficient is expressed as:

$$P_c = \frac{P}{\frac{1}{2}\rho_\infty V_\infty^3 S} \tag{8}$$

2.4 Aerodynamic Efficiency

The conventional wing aerodynamic efficiency is defined as:

$$\frac{C_L}{C_D} \tag{9}$$

For the CFJ wing, the ratio above still represents the pure aerodynamic relationship between lift coefficient and drag coefficient. However since CFJ active flow control consumes energy, the ratio above is modified to take into account the energy consumption of the micro-compressor. The formulation of the corrected aerodynamic efficiency for CFJ wings is:

$$(\frac{C_L}{C_D})_c = \frac{C_L}{C_D + P_c} \tag{10}$$

where P_c is the micro-compressor power coefficient defined in Eqn. 8 and C_L and C_D are the lift and drag coefficients of the CFJ wing. If the micro-compressor power coefficient is set to 0, this formulation returns to the aerodynamic efficiency of a conventional airfoil.

2.5 CFD Simulation Setup

The FASIP (Flow-Acoustics-Structure Interaction Package) CFD code is used to conduct the numerical simulation. The 3D Reynolds Averaged Navier-Stokes (RANS) equations with one-equation Spalart-Allmaras [13] turbulence model is used. A 3rd order WENO scheme for the inviscid flux [14, 15, 16, 17, 18, 19] and a 2nd order central differencing for the viscous terms [14, 18] are employed to discretize the Navier-Stokes equations. The low diffusion E-CUSP scheme used as the approximate Riemann solver suggested by Zha et al [15] is utilized with the WENO scheme to evaluate the inviscid fluxes. Implicit time marching method using Gauss-Seidel line relaxation is used to achieve a fast convergence rate [20]. Parallel computing is implemented to save wall clock simulation time [21]. The micro-compressor rotor flow is simulated in the rotating frame while the stator, the CFJ airfoil, and ducts are simulated in the stationary frame. In the rotating frame, the centrifugal and Coriolis forces are included as described in [22, 23].

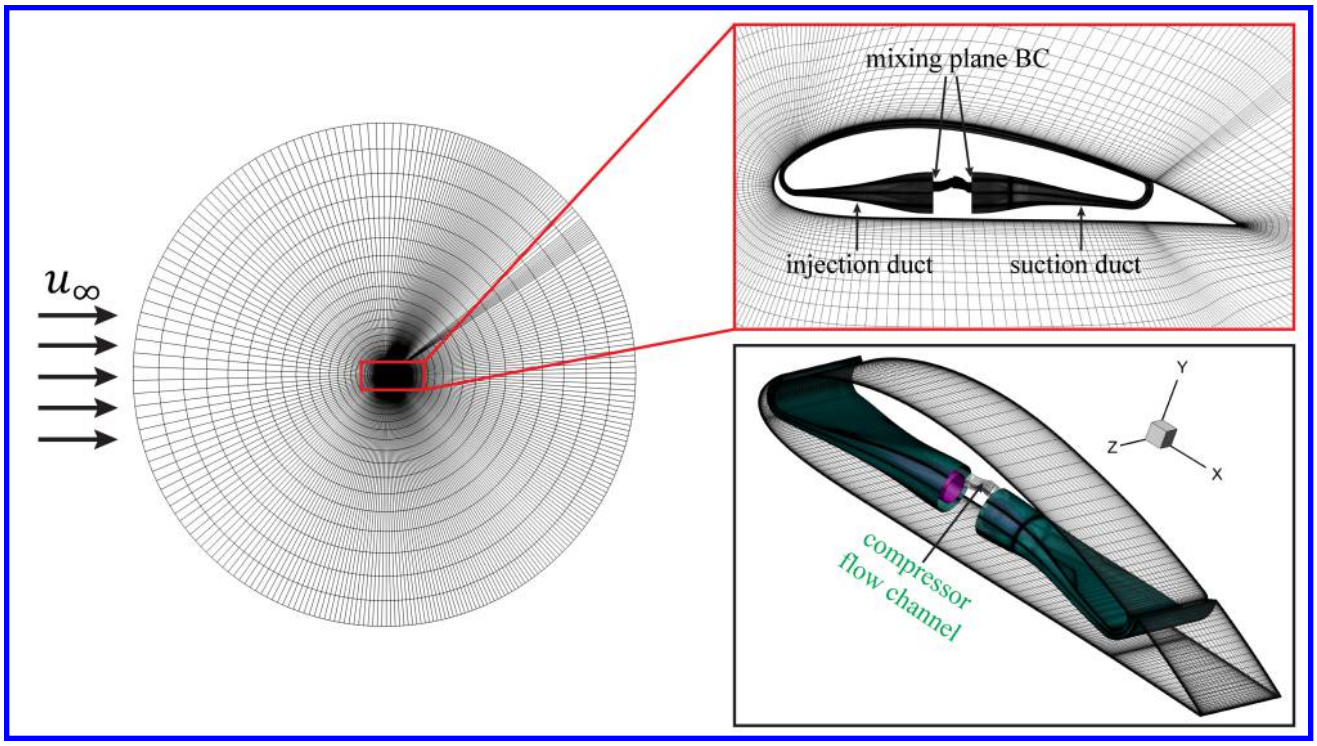

Figure 2: Computational mesh used in the current work.

2.6 Boundary Conditions

The 3rd order accuracy no slip condition is enforced on the solid surface with the wall treatment suggested in [24] to achieve the flux conservation on the wall. The computational mesh is shown in Fig. 2. Total pressure, total temperature and flow angles are specified at the upstream portion of the far field. Constant static pressure is applied at the downstream portion of the far field. Mixing plane boundary conditions are applied at the intersections of the ducts and the compressor. Symmetry boundary conditions are applied at the two sides in z-direction to ensure the effect of a segment of a 3D CFJ wing. The cross-section faces of the ducts are meshed using "H" topology while the parts around the airfoil are meshed using "O" topology. The total mesh size is 7.225 millions grid cells, split into 168 blocks for the parallel computation. The first grid point on the wing surface is placed at $y^+ \approx 1$.

3 Results

The parametric study results are presented in this section. The CFJ airfoil and micro-compressor performances are examined under different working conditions. The corresponding parameters of the CFJ airfoil and micro-compressor are listed in Table 1.

Table 1: Simulation parameters used in the current work.

Airfoil	CFJ-NACA-6421
Mach	0.3
AoA	$-5°\sim12°$
Compressor RPM	33,000
Compressor design RPM	30,000
Compressor design mass flow rate	0.165kg/s
Compressor design total pressure ratio	1.04
Compressor design efficiency	84.4%
Compressor Inner Diameter	40mm
Compressor Outer Diameter	64mm
# of stages	1
# of rotor blade set	13
# of stator blade set	15

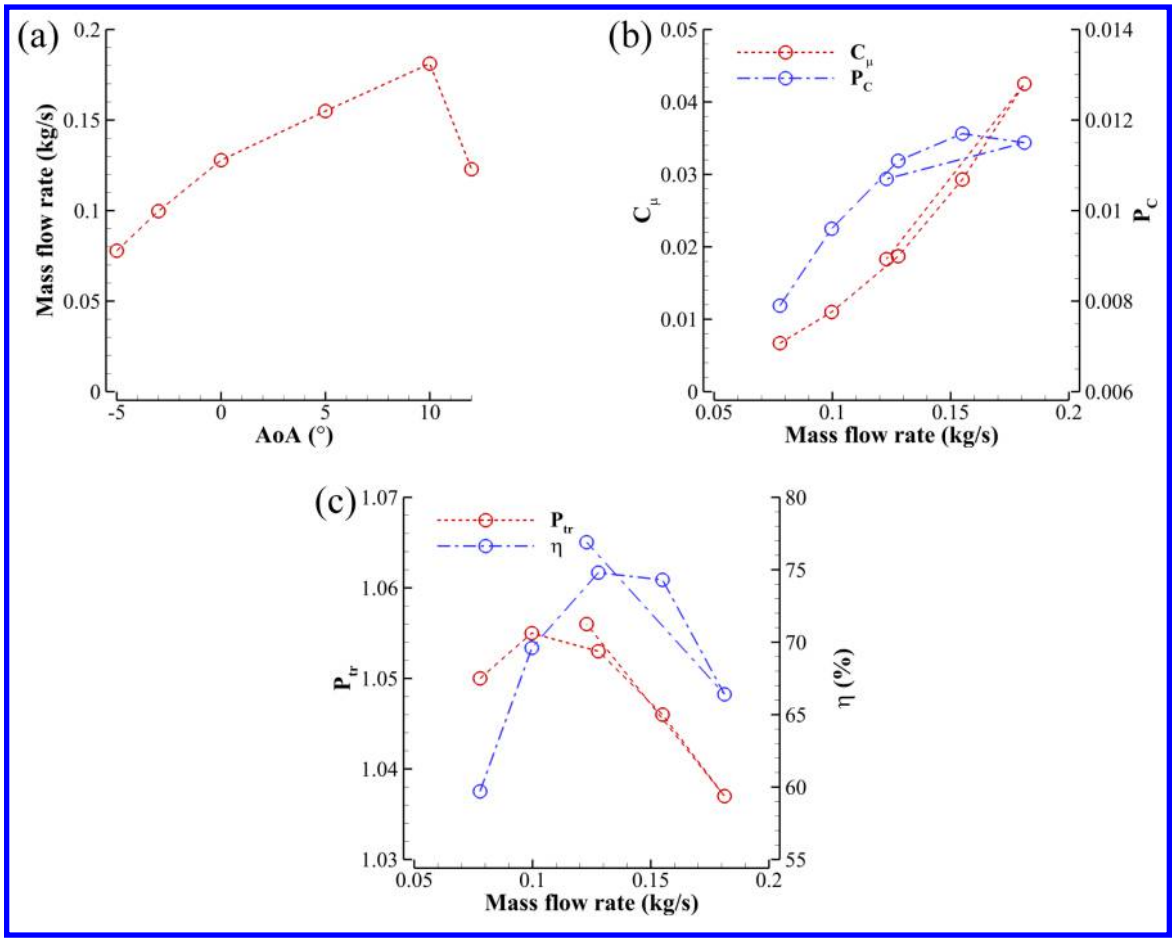

Figure 3: Aerodynamic performance of the micro-compressor, (a) AoA and $\dot{m}$; (b) C_μ and P_c; (c) P_{tr} and η.

Six cases (C1 - C6) are studied with fixed compressor RPM 33,000. Different compressor working points are

Table 2: Simulation results of the current work.

Cases	AoA	C_L	C_D	P_C	C_L/C_D	$(C_L/C_D)_c$	C_μ	P_{tr}	T_{tr}	$\dot{m}$ (kg/s)	η (%)
C1	$-5°$	0.167	0.0129	0.0079	13.0	8.0	0.0067	1.050	1.023	0.078	59.7
C2	$-3°$	0.410	0.0086	0.0096	47.6	22.5	0.0110	1.055	1.022	0.100	69.6
C3	$0°$	0.780	0.0064	0.0111	122.6	44.6	0.0187	1.053	1.020	0.128	74.8
C4	$5°$	1.304	0.0133	0.0117	98.2	52.3	0.0293	1.046	1.018	0.155	74.3
C5	$10°$	1.697	0.0355	0.0115	47.8	36.1	0.0425	1.037	1.016	0.181	66.4
C6	$12°$	0.917	0.1337	0.0107	6.9	6.3	0.0183	1.056	1.020	0.123	76.9

studied by changing the mass flow rate pass through the compressor, which is achieved by modifying the CFJ airfoil AoA. As shown in Fig. 3 (a), the compressor mass flow rate linearly increases with the rise of the CFJ airfoil AoA, except for the case C6, which presents airfoil stall due to too high AoA. Fig. 3 (b) shows the CFJ airfoil jet momentum coefficient C_μ and compressor power coefficient P_C at different compressor working points. We can see that C_μ increases with the rise of ~~compressor $\dot{m}$,~~ except for the case C6. The airfoil stall leads to the drop of the mass flow. For the compressor P_C, case C4 shows the largest power consumption. Fig. 3 (c) presents the compressor total pressure ratio and efficiency at different working points. It is clear to see that the compressor stalls for the case C1, which leads to the lowest efficiency $\eta = 59.7\%$. High efficiency points corresponds to a $\dot{m}$ around 0.15kg/s, which is close to the compressor design mass flow rate. It is worth noting that for high AoA case C6, the CFJ airfoil stalls before the compressor chokes. The stall of the airfoil decreases the mass flow passing through the compressor, which prevent the compressor from achieving higher mass flow.

The aerodynamic performance of the CFJ airfoil is shown in Fig. 4. We can see from the figure that C_L is almost linearly increased with the rise of airfoil AoA except for the case C6 due to the airfoil stall. Case C3 shows the maximum $C_L/C_D = 122.6$. Case C4 shows the maximum $(C_L/C_D)_c = 52.3$, which corresponds to the compressor efficiency $\eta = 74.3\%$

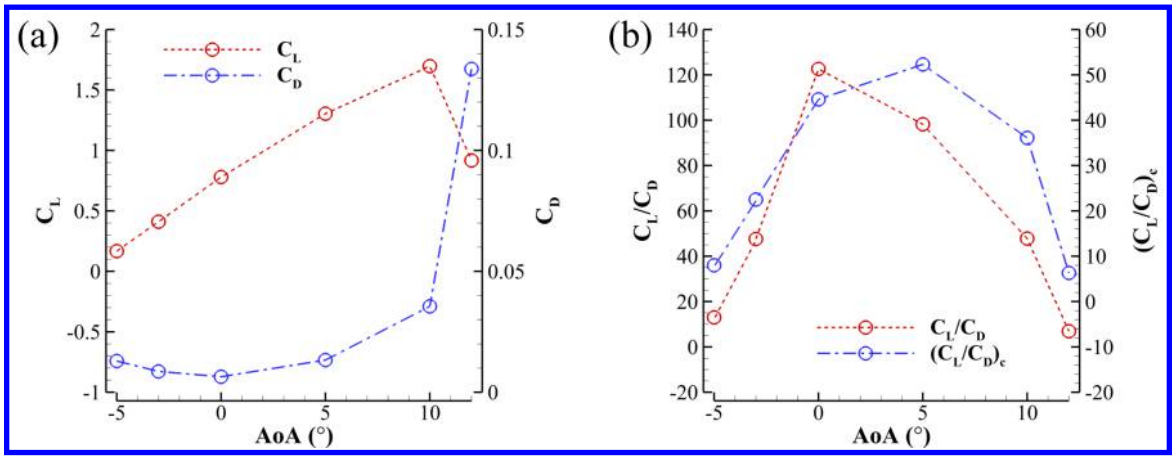

Figure 4: Aerodynamic performance of the CFJ airfoil, (a) C_L and C_D; (b) C_L/C_D and $(C_L/C_D)_c$.

The flow field around the CFJ airfoil at different compressor working points are described in the following. Case C1, C4, and C6 are chosen for the demonstration. The flow slices at the the mid span of the airfoils are shown in Fig. 5. The simulation results show well attached flow for the case C1 and C4, while large flow separation on the airfoil suction surface can be observed for the case C6, which suggests that the airfoil stalls. The flow separation decreases the static pressure near the suction duct inlet and limits the mass flow going through the compressor.

In addition, non-uniform flow can be observed inside the suction duct for the case C1, which suggests that the compressor stalls.

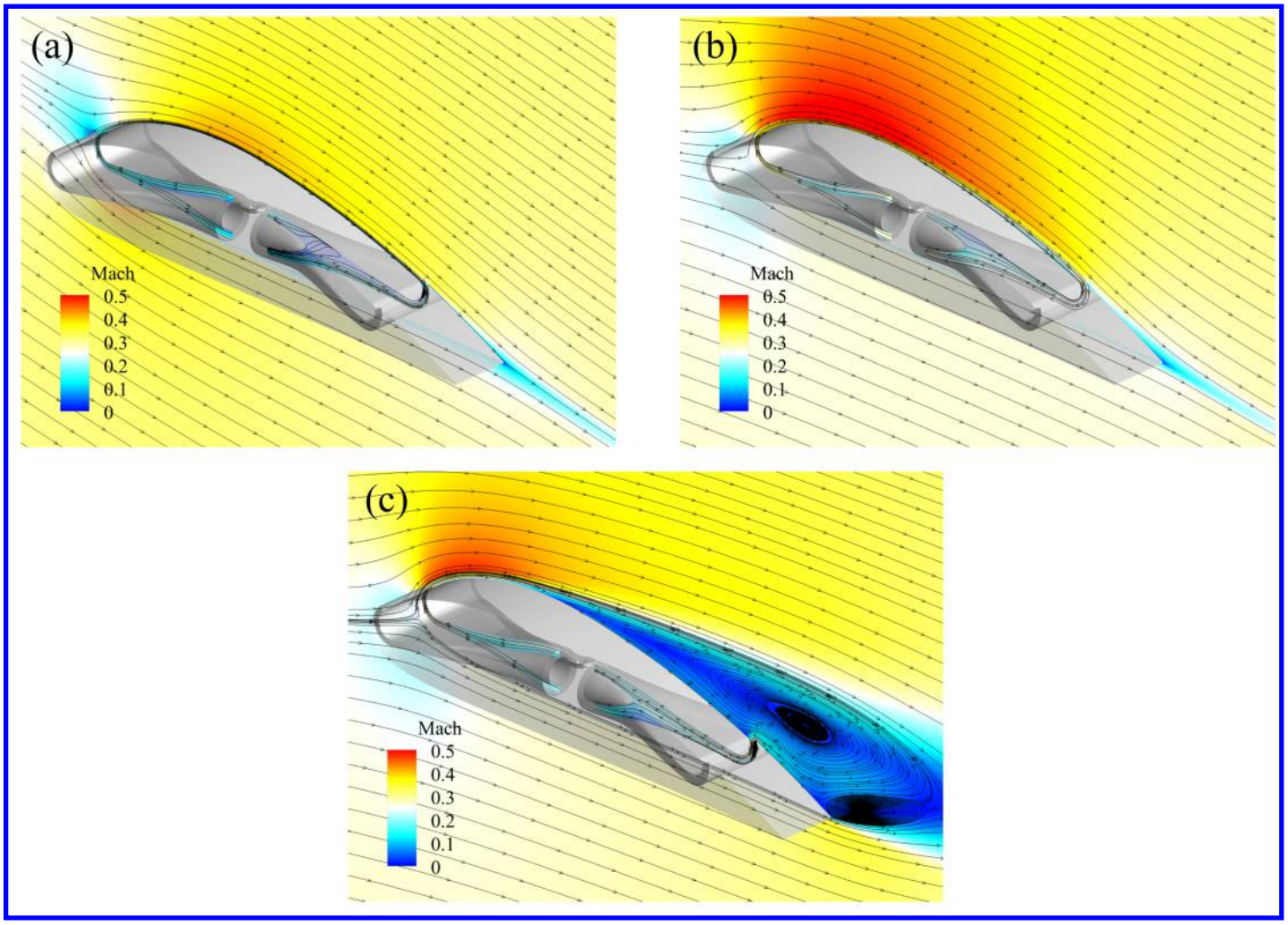

Figure 5: 2D flow slices at the mid span of the case C1, C4, and C6.

Blade to blade flow slices of the micro-compressor for the three cases are shown in Fig. 6. For the case C1, flow separation can be observed for both rotor and stator blades, which suggests that the compressor stalls. For the case C4 and C6, no flow separation can be observed for both cases. The compressor efficiency η is high (around 75%) for these two cases. Larger high speed zone near the rotor blade leading edge can be observed for the case C4 than the case C6 since the mass flow rate is greatly reduced for the case C6 due to the stall of the CFJ airfoil. The above study suggests that for large AoA cases that may lead to airfoil stall, the compressor RPM need to be increased to move the compressor operating line up to have higher mass flow rate and C_μ.

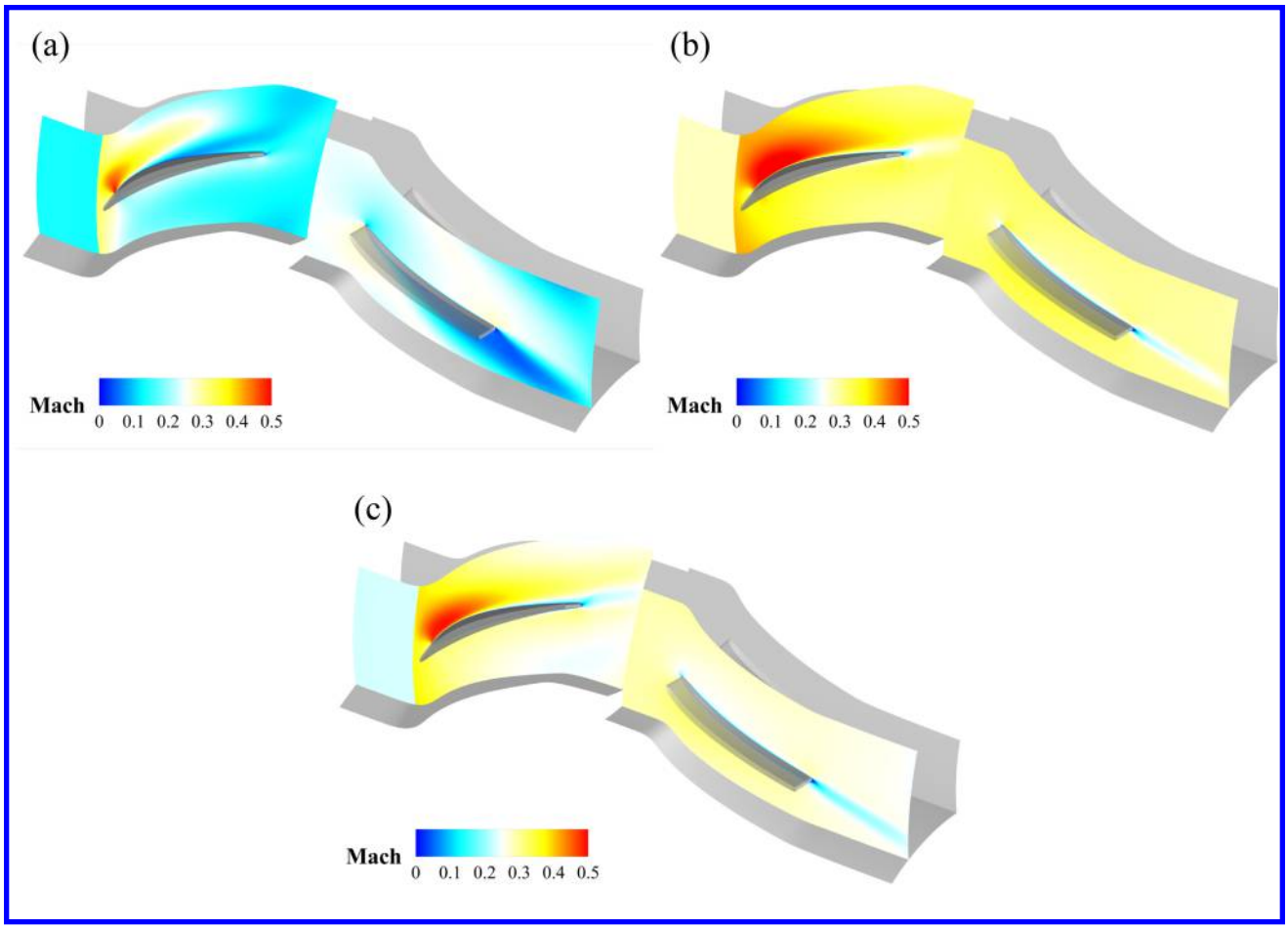

Figure 6: 3D micro-compressor blade to blade flow slices 0.74 blade span for the case C1, C4, and C6.

4 Conclusion

This paper presents the simulations of 3D Co-Flow Jet (CFJ) active flow control airfoil with an integrated micro-compressor. This is an important step to simulate the CFJ flow control airfoil by controlling the RPM of the micro-compressor actuator. The simulations are performed at freestream Mach number 0.3 to simulate the cruise condition of a general aviation electric aircraft. The airfoil used in this work is CFJ-NACA-6421. The simulations employ 3D RANS solver with Spalart-Allmaras (S-A) turbulence model, 3rd order WENO scheme for the inviscid fluxes, and 2nd order central differencing for the viscous terms.

The micro-compressor actuator is designed to achieve high efficiency at a required mass flow rate to maintain a desirable momentum coefficient (C_μ) of the CFJ airfoil at a certain flight condition. The aerodynamic performance, CFJ mass flow rate, energy expenditure, and 3D flow field are studied for the CFJ airfoil at different micro-compressor working points, which is achieved by fixing the compressor RPM and modifying the CFJ airfoil Angles of Attack (AoA). The results show that the compressor mass flow rate linearly increases with the rise of the CFJ airfoil AoA, except at a high AoA of 12°, which leads to the stall of the airfoil. When the AoA increases, the CFJ airfoil stalls before the compressor chokes. The stall of the airfoil decreases the mass flow passing through the compressor, which prevent the compressor from achieving higher mass flow. For the aerodynamic performance of the CFJ airfoil, the maximum C_L/C_D achieved is 122.6. The maximum $(C_L/C_D)_c$ achieved is 52.3, with the

compressor efficiency $\eta = 74.3\%$. The simulation results suggest that for large AoA leading to airfoil stall, the compressor RPM need to be increased to move the compressor operating line up to have higher mass flow rate and C_μ. The present study establishes a very important simulation tool, which can mimic the whole CFJ airfoil aerodynamic performance with integrated micro-compressor actuators to control the airfoil within a flight envelop at different operating conditions.

References

[1] G.-C. Zha and D. C. Paxton, "A Novel Flow Control Method for Airfoil Performance Enhancement Using Co-Flow Jet." *Applications of Circulation Control Technologies*, Chapter 10, p. 293-314, Vol. 214, Progress in Astronautics and Aeronautics, AIAA Book Series, Editors: Joslin, R. D. and Jones, G.S., 2006.

[2] G.-C. Zha, W. Gao, and C. Paxton, "Jet Effects on Co-Flow Jet Airfoil Performance," *AIAA Journal, No. 6,*, vol. 45, pp. 1222–1231, 2007.

[3] G.-C. Zha, C. Paxton, A. Conley, A. Wells, and B. Carroll, "Effect of Injection Slot Size on High Performance Co-Flow Jet Airfoil," *AIAA Journal of Aircraft*, vol. 43, 2006.

[4] G.-C. Zha, B. Carroll, C. Paxton, A. Conley, and A. Wells, "High Performance Airfoil with Co-Flow Jet Flow Control," *AIAA Journal*, vol. 45, 2007.

[5] Wang, B.-Y. and Haddoukessouni, B. and Levy, J. and Zha, G.-C., "Numerical Investigations of Injection Slot Size Effect on the Performance of Co-Flow Jet Airfoil," *Journal of Aircraft*, vol. Vol. 45, No. 6,, pp. pp.2084–2091, 2008.

[6] B. P. E. Dano, D. Kirk, and G.-C. Zha, "Experimental Investigation of Jet Mixing Mechanism of Co- Flow Jet Airfoil." AIAA-2010-4421, 5th AIAA Flow Control Conference, Chicago, IL, 28 Jun - 1 Jul 2010.

[7] B. P. E. Dano, G.-C. Zha, and M. Castillo, "Experimental Study of Co-Flow Jet Airfoil Performance Enhancement Using Micro Discreet Jets." AIAA Paper 2011-0941, 49th AIAA Aerospace Sciences Meeting, Orlando, FL, 4-7 January 2011.

[8] A. Lefebvre, B. Dano, W. Bartow, M. Fronzo, and G. Zha, "Performance and energy expenditure of coflow jet airfoil with variation of mach number," *Journal of Aircraft*, vol. 53, no. 6, pp. 1757–1767, 2016.

[9] A. Lefebvre, G-C. Zha, "Numerical Simulation of Pitching Airfoil Performance Enhancement Using Co-Flow Jet Flow Control," *AIAA paper 2013-2517*, June 2013.

[10] A. Lefebvre, G-C. Zha, "Cow-Flow Jet Airfoil Trade Study Part I : Energy Consumption and Aerodynamic Performance," *32nd AIAA Applied Aerodynamics Conference, AIAA AVIATION Forum, AIAA 2014-2682*, June 2014.

[11] A. Lefebvre, G-C. Zha, "Cow-Flow Jet Airfoil Trade Study Part II : Moment and Drag," *32nd AIAA Applied Aerodynamics Conference, AIAA AVIATION Forum, AIAA 2014-2683*, June 2014.

[12] Y. Ren and G. Zha, "Design of injection and suction ducts for co-flow jet airfoils with embedded micro-compressor actuator," in *AIAA Paper 2018-3062, 2018 Flow Control Conference*, p. 3062, 2018.

[13] P. R. Spalart and S. R. Allmaras, "A one-equation turbulence model for aerodynamic flows," in *30th Aerospace Sciences Meeting and Exhibit, Aerospace Sciences Meetings, Reno, NV, USA, AIAA Paper 92-0439*, 1992.

[14] Y.-Q. Shen and G.-C. Zha, "Large Eddy Simulation Using a New Set of Sixth Order Schemes for Compressible Viscous Terms ," *Journal of Computational Physics*, vol. 229, pp. 8296–8312, 2010.

[15] Zha, G.C., Shen, Y.Q. and Wang, B.Y., "An improved low diffusion E-CUSP upwind scheme ," *Journal of Computer and Fluids*, vol. 48, pp. 214–220, Sep. 2011.

[16] Y.-Q. Shen and G.-Z. Zha , "Generalized finite compact difference scheme for shock/complex flowfield interaction," *Journal of Computational Physics*, vol. doi:10.1016/j.jcp.2011.01.039, 2011.

[17] Shen, Y.-Q. and Zha, G.-C. and Wang, B.-Y., " Improvement of Stability and Accuracy of Implicit WENO Scheme," *AIAA Journal*, vol. 47, No. 2, pp. 331–344, 2009.

[18] Shen, Y.-Q. and Zha, G.-C. and Chen, X.-Y., " High Order Conservative Differencing for Viscous Terms and the Application to Vortex-Induced Vibration Flows," *Journal of Computational Physics*, vol. 228(2), pp. 8283–8300, 2009.

[19] Shen, Y.-Q. and Zha, G.-C. , " Improvement of the WENO Scheme Smoothness Estimator," *International Journal for Numerical Methods in Fluids*, vol. DOI:10.1002/fld.2186, 2009.

[20] G.-C. Zha and E. Bilgen, "Numerical Study of Three-Dimensional Transonic Flows Using Unfactored Upwind-Relaxation Sweeping Algorithm," *Journal of Computational Physics*, vol. 125, pp. 425–433, 1996.

[21] B.-Y. Wang and G.-C. Zha, "A General Sub-Domain Boundary Mapping Procedure For Structured Grid CFD Parallel Computation," *AIAA Journal of Aerospace Computing, Information, and Communication*, vol. 5, No.11, pp. 2084–2091, 2008.

[22] H. Im and G. Zha, "Investigation of flow instability mechanism causing compressor rotor-blade nonsynchronous vibration," *AIAA journal*, vol. 52, no. 9, pp. 2019–2031, 2014.

[23] P. Patel and G. Zha, "Investigation of mixed micro-compressor casing treatment using non-matching mesh interface," in *Turbo Expo: Power for Land, Sea, and Air*, vol. 58714, p. V008T26A013, American Society of Mechanical Engineers, 2019.

[24] Y.-Q. Shen, G.-C. Zha, and B.-Y. Wang, "Improvement of Stability and Accuracy of Implicit WENO Scheme ," *AIAA Journal*, vol. 47, pp. 331–344, 2009.